Vol. 24, No. 1(2025) Mat24409
Revista Mexicana de Ingeniería Química

Nickel electrodeposition from an aqueous solution of ammonium chloride onto a Highly Oriented Pyrolytic Graphite (HOPG) electrode: A kinetic and morphological study

Electrodeposición de níquel a partir de una solución acuosa de cloruro de amonio sobre un electrodo de grafito pirolítico altamente orientado (HOPG): Un estudio cinético y morfológico

L.H. Mendoza-Huizar*
Área Académica de Química. Ciudad del Conocimiento. Universidad Autónoma del Estado de Hidalgo, Carretera Pachuca-Tulancingo km. 4.5, CP. 42184 Mineral de la Reforma, Hidalgo, México.
Received: August 31, 2024; Accepted: November 12, 2024

Abstract
In this study, an electrochemical investigation was conducted on the electrodeposition of nickel onto a Highly Oriented Pyrolytic Graphite (HOPG) electrode from an ammoniacal solution containing 0.01 M $NiCl_2$ and 0.1 M NH_4Cl. The potential range in which nickel can be electrodeposited was determined by a cyclic voltammetric study, which also made it possible to assess the charge transfer coefficients related to the reduction and oxidation processes. A kinetic analysis of the nucleation and growth of nickel was also carried out using chronoamperometry. The current density transients (CDTs) derived from this technique were modeled through a kinetic mechanism involving three distinct contributions: (a) two-dimensional instantaneous nucleation, (b) three-dimensional nucleation limited by mass transfer, and (c) a proton reduction process. Nonlinear fitting of the CDTs indicated that both the nucleation rate (A) and the number of active nucleation sites (N_0) increased with the applied potential. Furthermore, the analysis of the contributions to the CDTs showed that, on average, 7.9% of the applied electric charge is consumed by the nucleation and growth process, while the remainder is used for proton reduction. The average Gibbs free energy (ΔG) calculated for the formation of a stable nucleus was 1.2×10^{-20} J nucleus^{-1}. Additionally, Scanning Electron Microscopy (SEM) analysis revealed the presence of spherical nickel particles dispersed on the surface, with diameters ranging from 60 nm to 235 nm.
Keywords: nickel, electrodeposition, kinetic, SEM.

Resumen
En este estudio, se realizó una investigación electroquímica de la electrodeposición de níquel sobre un electrodo de grafito pirolítico altamente orientado (HOPG) a partir de una solución amoniacal que contenía 0.01 M $NiCl_2$ y 0.1 M NH_4Cl. El rango de potencial en el que puede electrodepositarse el níquel se determinó mediante un estudio de voltamperometría cíclica, que también permitió evaluar los coeficientes de transferencia de carga relacionados con los procesos de reducción y oxidación. También, se llevó a cabo un análisis cinético de la nucleación y el crecimiento del níquel mediante la técnica de cronoamperometría. Los transitorios de densidad de corriente (CDTs) derivados a partir de esta técnica se modelaron mediante un mecanismo cinético que implica tres contribuciones distintas: (a) una nucleación instantánea bidimensional, (b) una nucleación tridimensional limitada por transferencia de masa, y (c) un proceso de reducción de protones. El ajuste no lineal de los CDTs indicó que tanto la velocidad de nucleación (A) como el número de sitios activos de nucleación (N_0) aumentaban con el potencial aplicado. Además, el análisis de las contribuciones a los CDTs mostró que, en promedio, el 7.9% de la carga eléctrica aplicada se consume en el proceso de nucleación y crecimiento, mientras que el resto se utiliza en la reducción de protones. La energía libre de Gibbs (ΔG) calculada para la formación de un núcleo estable fue de 1.2×10^{-20} J núcleo^{-1}. Además, el análisis por microscopía electrónica de barrido (SEM) reveló la presencia de partículas esféricas de níquel dispersas en la superficie, con diámetros comprendidos entre 60 nm y 235 nm.
Palabras clave: níquel, electrodeposición, cinética, SEM.

*Corresponding author. *E-mail*: hhuizar@uaeh.edu.mx;
https://doi.org/10.24275/rmiq/Mat24409
ISSN:1665-2738, *issn-e*: 2395-8472

1 Introduction

Nickel is widely used in industrial and commercial applications, it is used to improve the corrosion resistance of base metals such as steel (Cano, Romero, & Cubillos, 2023; Ruiz-Vela, Rodríguez-Vázquez, Gudiño-Pérez, Sánchez-Ramírez, & Montes-Rodríguez, 2023), and to provide a protective coating on mechanical components (Francis, 2023). Also, nickel is valued for its electrical conductivity, and wear resistance in the manufacture of electrical and electronic components. Nickel is also used in electrocatalysis (Huo *et al*., 2022; Putri *et al*., 2024; Vij *et al*., 2017), batteries fabrication (Bernal Lopez & Ustarroz, 2021; Cuevas-González, Monterrubio-Badillo, & Cuenca-Álvarez, 2018; Rehman *et al*., 2022), surface decoration and finishing, enhancing the aesthetic appeal and durability of products such as jewelry, faucets, and kitchen accessories (Di Bari, 2011; Dubpernell, 2006).

In the field of electrocatalysis, nickel as nanoparticles is widely used as catalysts for energy-Related Applications such as Oxygen Reduction (Vij *et al*., 2017), Oxygen Evolution, and Hydrogen Evolution Reactions (Huo *et al*., 2022), because of its high catalytic activity (Wang, Williamson, Dawson, & Bimbo, 2023), cost-effectiveness, and excellent stability (Vij *et al*., 2017). These nickel nanomaterials can be fabricated by multiple methods such as chemical reduction, photochemical synthesis, and ionothermal synthesis, and electrodeposition, among others (Mernissi Cherigui *et al*., 2017). However, electrodeposition offers several advantages since it permits the growth of the nanoparticles directly on the support of interest without the need for surfactants and allows obtaining highly electroactive nanostructures (Li *et al*., 2013). Although nickel electrodeposition has been extensively studied on different substrates (Abyaneh, Visscher, & Barendrecht, 1983; Ni *et al*., 2022; Skibińska, Semeniuk, Kutyła, Jędraczka, & Zabiński, 2021; Sotskaya, Sapronova, & Dolgikh, 2014; Zheng, Cao, & Zheng, 2007; Zhu, Katayama, & Miura, 2014), there is growing interest in its application on carbon-based surfaces due to its ability to enhance reactivity in a cost-effective manner (Bernal Lopez & Ustarroz, 2021). Materials such as graphene and carbon nanotubes exhibit unique characteristics that enhance nickel's catalytic performance by influencing the morphology and size of deposited particles, thereby impacting catalyst reactivity. Moreover, the electrodeposition of nickel on carbon substrates from aqueous solutions has been investigated using various buffers such as phosphate (Cheng, Wu, Chen, Zhou, & Wu, 2011), sulfates (Jin *et al*., 2012), or acetate (Kireev & Frolov, 2021). In these, studies by Torabi *et al*. (Torabi & Dolati, 2010) and Grujicic *et al*.(Grujicic & Pesic, 2006) have explored different aspects of nickel electrodeposition mechanisms from sulfate solutions, highlighting factors such as nucleation and growth processes. Thus, it was found that nickel electrodeposition follows an instantaneous nucleation mechanism with a 3D growth (Torabi & Dolati, 2010), but nickel is also electrodeposited through a progressive nucleation mechanism from aqueous sulfate solution at different values of pH (Grujicic & Pesic, 2006). Here it is important to mention that aqueous baths for nickel electrodeposition present challenges including low current efficiency, stringent process control, and complexity of bath and additives (Abbott, Ballantyne, Harris, Juma, & Ryder, 2015; Mernissi Cherigui *et al*., 2017), making them less attractive despite their low environmental impact. Moreover, electrodeposits obtained from aqueous chloride solutions are reported to be fragile and prone to corrosion (Francis, 2023; Huo *et al*., 2022). However, homogeneous conical nanostructures of nickel can be synthesized from aqueous ammoniacal solutions, with the presence of NH_4Cl being crucial for achieving a uniform nano-cone array (Ni *et al*., 2022; Skibińska *et al*., 2021). This uniformity can be attained by controlling various parameters, including substrate preparation, plating bath composition, and electrodeposition conditions (Skibińska *et al*., 2021). But, kinetic studies related to these chloride solutions are relatively sparse, despite the well-established fact that the properties of electrodeposits depend on nucleation and growth processes (Alemu, Assresahegn, & Soreta, 2014). Thus, there is limited research on the kinetic parameters of nickel electrodeposition from chloride solutions, despite their potential advantages in terms of reduced environmental impact. This limitation has also hindered research in the electrocatalyst field, where nickel nanostructures obtained from aqueous chloride media could prove valuable. Thus, a kinetic and morphological study of nickel deposition on highly oriented pyrolytic graphite (HOPG) from chloride solutions would provide insight into the nickel deposition mechanism in such aqueous plating baths. We believe that these studies are important for controlling the morphology and properties of nickel deposits, with potential applications in the field of electrocatalysis.

2 Methodology

Nickel electrodeposition onto HOPG was carried out from an aqueous solution containing 10^{-2} M of $NiCl_2$ and 0.1 M NH_4Cl at pH 7.0 (natural pH). All solutions were prepared using analytical grade reagents with ultra-pure water (Millipore-Q system) and deoxygenated by bubbling N_2 for 15

minutes before each experiment. A graphite bar with an exposed area greater than the working electrode was used as the counter electrode. A saturated silver electrode (Ag/AgCl) served as the reference electrode, and all measured potentials are referenced to this scale. The electrochemical experiments were conducted using an EPSILON potentiostat connected to a personal computer running BASI EPSILON EC software for experiment control and data acquisition. To assess the electrochemical behavior of the electrode in the electrodeposition bath, cyclic voltammetry was performed within the potential range of 0.600 to -1.300 V. The kinetic mechanism of nickel deposition onto HOPG was investigated under potentiostatic conditions through analysis of the experimental potentiostatic current density transients obtained using the potential step technique. The potential electrode perturbation always commenced at 0.600 V, as this initial potential allows the system to reach an optimal equilibrium state before measurement. Next, the potential step was then applied as described in this study.

3 Results and discussion

3.1 Voltamperometric study

Figure 1 depicts a typical voltammogram obtained for HOPG/10^{-2} M $NiCl_2$ + 0.1 M NH_4Cl system. During the direct scan, peak A is observed at -1.018 V, corresponding to the reduction of Ni^{2+}, according to the following reaction:

$$[Ni(H_2O)_6]^{2+} + 2e^- \rightarrow Ni^0 + 6H_2O \qquad (1)$$

The equilibrium potential for the latter reaction, as reported in the literature, is -0.257 V vs SHE (-0.454 V vs Ag/AgCl electrode) (Dean, J, 1999). When the scan is inverted to the anodic region, a crossover potential (E_{C1}) is detected at -1.251 V. This kind of crossover has been associated with the metal deposition onto substrates of different nature (Danaee, 2013). Another crossover (E_{C2}) at -0.45 V with zero current was recorded, which can be associated with the system's equilibrium potential. Note this value is very close to the -0.454 V reported in the literature for reaction (1). In the anodic region, peaks B and D are observed at -0.377 V and 0.147 V, respectively. Peak B has been related to the anodic formation of $Ni(OH)_{ads}$, while peak D is associated with the dissolution of nickel deposited during the forward scan. (Mernissi Cherigui *et al*., 2017).

It is common to determine the limiting control of the electrodeposition process by plotting the current value associated with the peak A vs. $\nu^{1/2}$ (ν = scan rate) (Berzins & Delahay, 1953). However, the formation

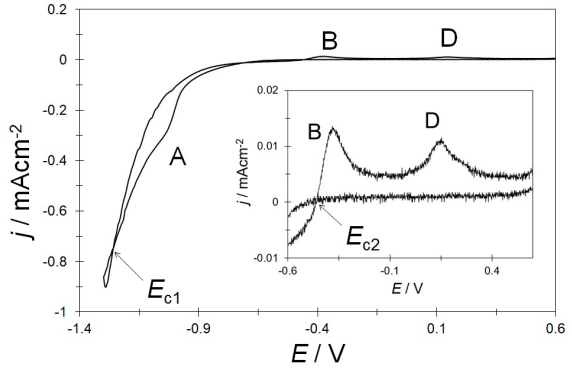

Figure 1. A typical cyclic voltammogram obtained from the HOPG/10^{-2} M $NiCl_2$ + 0.1 M NH_4Cl system. The potential scan rate was started at 0.600 V toward the negative direction with a potential scan rate of 10 mV s^{-1}.

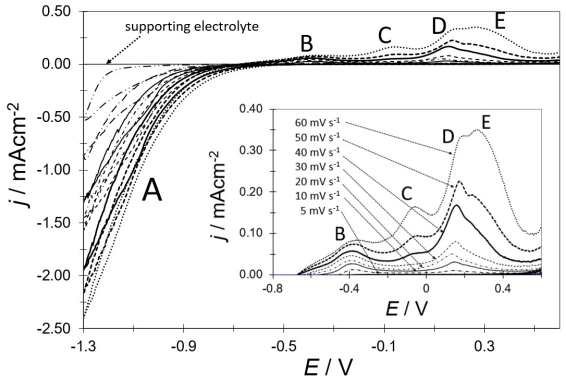

Figure 2: Cyclic voltammograms obtained from the HOPG/10^{-2} M $NiCl_2$ + 0.1 M NH_4Cl system at 25 °C at different scan rates.

of well-defined peak A was not possible at scan rates bigger than 30 mV s^{-1} (see Figure 2), which suggests the presence of an additional process for the nucleation and growth of nickel onto the HOPG substrate, which may be due to the proton reduction process (Rios-Reyes, Mendoza-Huizar, & Rivera, 2010). The anodic peaks B, C, D, and E were recorded at -0.4 V, -0.06 V, 0.172 V, and 0.30 V, respectively. Peaks B, C, -0.4, and -0.06 V have been attributed to the anodic formation of $Ni(OH)_{ads}$ and $Ni(OH)_{2ads}$ (Mernissi Cherigui *et al*., 2017), while peaks D and E to the anodic process correspond to the stripping of nickel deposited during the direct scan (Jamil, Ruiz-Trejo, & Brandon, 2017; Mernissi Cherigui *et al*., 2017).

Kinetic parameters associated with the oxidation and reduction processes were evaluated according to Tafel equations (Tafel, 1905), as shown in equations (2) and (3):

$$\ln j_c = \ln j_0 + \frac{(1-\alpha_c)F}{RT}\eta \qquad (2)$$

$$\ln j_a = \ln j_0 + \frac{\alpha_c F}{RT}\eta \qquad (3)$$

In these equations, j_c and j_a represent the cathodic and anodic current densities, respectively; j_0 is the

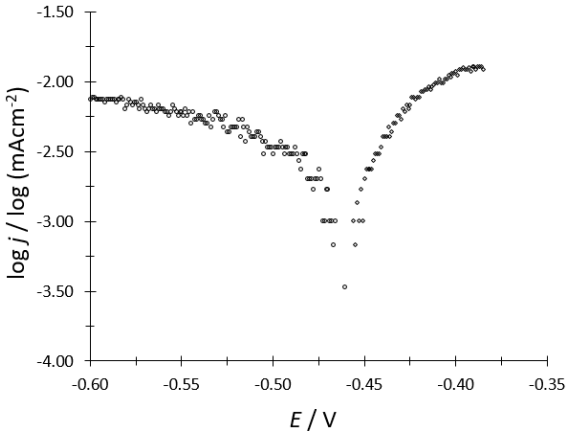

Figure 3. Tafel plots obtained from a voltamperogram of the HOPG/10^{-2} M $NiCl_2$ + 0.1 M NH_4Cl system at 25°C, at a scan rate of 5 mV s^{-1}.

exchange current density; α_c is the cathodic transfer coefficient. The plot of the logarithm of the current versus the potential applied near the equilibrium point is shown in Figure 3. The data for the anodic and cathodic branches were obtained from a voltamperogram recorded at a scan rate of 5 mV s^{-1}. Fitting the linear portion of these branches to the Tafel equations yielded a cathodic transfer coefficient of 0.64, while the anodic transfer coefficient was 0.36.

3.2 Chronoamperometric study

Detailed information about the electrocrystallization process can be obtained from potentiostatic deposition. Thus, from a chronoamperometric study, it is possible to determine nucleation parameters such as nucleation rate values and the density number of active nucleation sites, which characterize the nucleation and growth processes. In Figure 4, a set of current density

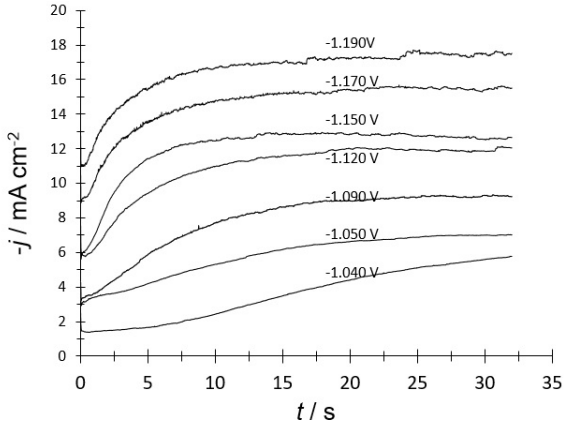

Figure 4. A set of transients obtained from HOPG/10^{-2} M $NiCl_2$ + 0.1 M NH_4Cl system by means of the potential step technique for different potential step values (V) indicated in the figure. In all the cases, the initial potential was 0.600 V.

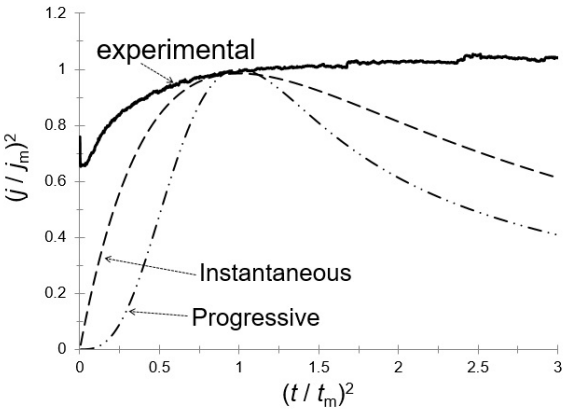

Figure 5. Comparison of an experimental transient normalized (through the coordinates of its respective local maximum (t_m, j_m), with the theoretical nondimensional curves corresponding to 3D instantaneous nucleation (Eq. (4)) and 3D progressive nucleation (Eq. (5)).

transients (CDTs) recorded onto HOPG electrode at different potentials by the step potential technique is depicted. Note that CDTs obtained on HOPG do not show the presence of a well defined peak. This behavior has been associated with a system in which the current associated with the nucleation process is overlapped with a proton reduction process (Rios-Reyes *et al*., 2010).

By using the criteria established by Sharifker *et al*., it is possible to classify the nucleation and growth process of nickel as progressive or instantaneous (Scharifker & Hills, 1983). In this procedure, the experimental CDTs in a nondimensional form are obtained by plotting $j^2/j_m{}^2$ vs. t/t_m, and then they are compared with those theoretically generated from Eqs. (4) and (5) for instantaneous and progressive nucleation, respectively (Scharifker & Hills, 1983).

$$\frac{j^2}{j_m^2} = 1.9542\left(\frac{t}{t_m}\right)^{-1}\left\{1-\exp\left[-1.2564\left(\frac{t}{t_m}\right)\right]\right\}^2 \quad (4)$$

$$\frac{j^2}{j_m^2} = 1.2254\left(\frac{t}{t_m}\right)^{-1}\left\{1-\exp\left[-2.3367\left(\frac{t}{t_m}\right)\right]\right\}^2 \quad (5)$$

In Figure 5, it is shown a comparison of the theoretical dimensionless transients, generated by equations (4) and (5) with the experimental dimensionless current transients obtained from HOPG/10^{-2} M $NiCl_2$ + 0.1 M NH_4Cl. It is clear that equations (4) and (5) could not predict the general behavior of CDTs.

The behavior of the CDTs depicted in Figure 5 may be associated with a reduction proton process that is coupled to a nucleation and growth process. (Rios-Reyes *et al*., 2010). Palomar-Pardavé *et al*. have proposed that, for systems in which the proton reduction process is occurring simultaneously with the diffusion-limited 3D growth of metallic nuclei centers, the overall current density is given by equation (6) (Palomar-Pardavé, Scharifker, Arce, & Romero-

Romo, 2005):

$$j_{3D}(t) = [P_1^* + P_4(t-n)^{-1/2}] \left\{1 - \exp\left[(t-n) - \frac{1-\exp(-P_3(t-n))}{P_3}\right]\right\} \quad (6)$$

$$P_1^* = P_1\left(\frac{2cM}{\pi\rho}\right)^{1/2}, \quad (7)$$

$$P_1 = z_{PR}Fk_{PR}, \quad (8)$$

$$P_2 = N_0\pi kD, \quad (9)$$

$$P_3 = A, \quad (10)$$

$$P_4 = \frac{2FD^{1/2}c}{\pi^{1/2}}, \quad (11)$$

$$k = \left(\frac{8\pi c}{\rho}\right)^{1/2} \quad (12)$$

where $z_{PR}F$ is the molar charge transferred during the proton reduction process, k_{PR} is the rate constant of the proton reduction reaction, N_0 is the density number of active nucleation sites, A is the nucleation rate, D is the diffusion coefficient, F is the Faraday's constant, n is the induction time, and all other parameters have their electrochemical conventional meanings. However, at initial times, equation (6) is unable to adequately predict the transients shown in Figure 4, suggesting the presence of an additional process not accounted for in that equation. While the charge of the double layer must be considered at shorter times (Hölzle, Retter, & Kolb, 1994), this contribution occurs within a few milliseconds and becomes negligible thereafter (Whiston, Bilec, & Schaefer, 2015). In our case, a 2D instantaneous contribution (Armstrong & Harrison, 1969), combined with equation (6), could adequately predict the full transient. Therefore, it is proposed that the total contribution to the transient should be given by:

$$j_T = j_{2D-i} + j_{3D} \quad (13)$$

where

$$j_{2D-i}(t) = k_1 e^{-k_2 t} \quad (14)$$

where $k_1 = q_{mon}S^2D$, $k_2 = \pi S^2 D N_0$, in these equations q_{mon} is the charge density associated with formation of the monolayer, S is a constant controlled by the potential, D is the diffusion coefficient of the metal ion and N_0 is the number density of active sites. Here, $k_1 = k_2 Q_{nucl}$ and Q_{nucl} is the charge density due to the 2D nucleation process. Figure 6 shows a typical comparison of the reduction experimental current transients with the theoretically generated by non-linear fitting of experimental data to Eq. (13). It can be observed that the model expressed by this equation adequately accounts for the behavior of experimental transients. The physical parameters obtained from the adjustments to Eq. (13) are summarized in Table 1. It can be observed that the values of k_{PR}, A, and N_0 increase with the applied potential, while an average diffusion coefficient of 1.22×10^{-6} cm^2s^{-1} was obtained. A similar trend was observed for Ni electrodeposition on a copper substrate (Sotskaya *et al*., 2014). But the nucleation rate and the k_{PR} values are lower for HOPG compared to the copper electrode (Sotskaya *et al*., 2014). Note that in the analyzed potential range, the contributions to the CDTs show that, on average, 7.9% of the applied electric charge is consumed by the nucleation and growth process, while the remaining portion is utilized for proton reduction. Thus, the total charge contributing to the nucleation process is low compared to the charge related to the hydrogen evolution process, suggesting low efficiency, as reported in the literature for aqueous systems (Abbott *et al*., 2015).

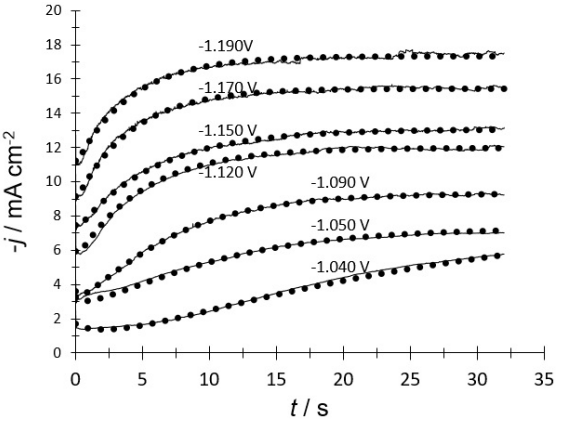

Figure 6. Comparison between experimental current density transients (___) recorded at different applied potential with the respective theoretical transient (●●●) generated by non-linear fitting of Eq. (13).

3.3 Analysis of the kinetic parameters

Also, from the nucleation rate values reported (see Table 1), it is possible to calculate the Gibbs free energy of nucleation employing the next equation (Group, 1985a; Mostany, Mozota, & Scharifker, 1984; Serruya, Mostany, & Scharifker, 1999):

$$A = k_3 \exp\left(-\frac{\Delta G}{K_B T}\right) = k_3 \exp\left(-\frac{k_4}{\eta^2}\right) \quad (15)$$

where ΔG is the Gibbs free energy of nucleation, J $nucleus^{-1}$; K_B is the Boltzmann constant ($1.38066X10^{-23}$ J mol^{-1}), $k_3 = N_0\omega_{n+c}\Gamma$, where, ω_{n+c} is the frequency of attachment of single atoms to the critical nucleus, Γ is the non-equilibrium Zeldovich factor, and depends exponentially on the overpotential (η) (Milchev, 2002), where η is evaluated as the difference between the applied potential and the equilibrium potential. On the other hand, $k_4 = -(16\pi\gamma^3M^2\phi(\theta)/3\rho^2z^2F^2kT)$, where γ is the interfacial tension of the nucleus with its mother phase is a function of the contact angle between the nucleus and the substrate (Milchev, 2002). In order to calculate

Table 1. Potential dependence for the nucleation parameters during Ni electrodeposition on a HOPG electrode from an aqueous solution containing 10^{-2} M of $NiCl_2$ + 0.1 M NH_4Cl at pH 7.0 (natural pH). The values were obtained from the best-fit parameters found through the fitting process of the experimental *j-t* plots using Eq. (13). Also the electric charge contributions to the processes involved are reported.

E/V	A/ s^{-1}	$N_0 \times 10^{-6}$ / cm^{-2}	$K_{PR} \times 10^{8}$ / mol cm^2	Q_{Total} / C cm^{-2}	$Q_{2D-i} + Q_{3D}$ %	Q_{H2} %
-1.04	2.01	1.31	9.10	0.112	4.30%	95.70%
-1.05	2.18	3.92	7.50	0.185	2.80%	97.20%
-1.09	2.70	5.52	9.59	0.253	5.30%	94.70%
-1.12	4.29	6.41	12.35	0.349	9.30%	90.70%
-1.15	6.25	12.68	13.15	0.386	9.10%	90.90%
-1.17	10.29	7.74	15.93	0.467	8.90%	91.10%
-1.19	12.85	9.40	17.91	0.528	12.20%	87.80%

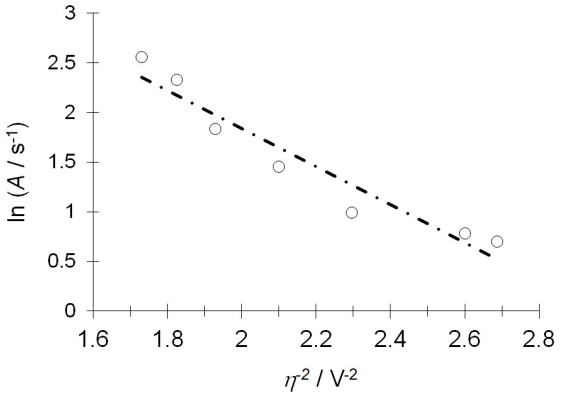

Figure 7. In A vs η^{-2} plot, used to calculate the Gibbs energy of nucleation according to Eq. (13). The dashed straight line corresponds to the linear fit of the experimental data.

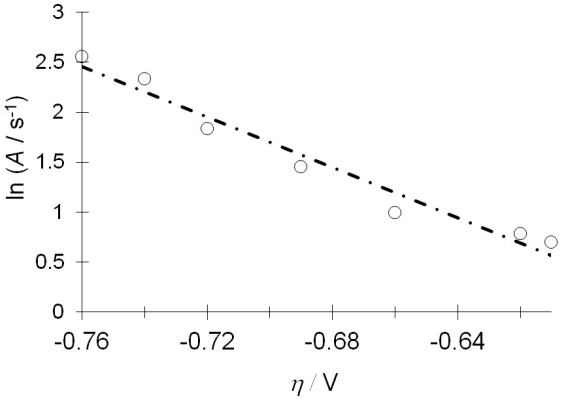

Figure 8. In A vs η plot, used to calculate the critical size of Ni nucleus according to Eq. (15). The dashed straight line corresponds to the linear fit of the experimental data.

the value of Gibbs free energy of nucleation from experimental transients, an ln$A$ vs. η^{-2} plot can be constructed according to Eq. (15), and then from the slope k_4 of the observed linear relationship, ΔG could be calculated at each particular overpotential by using the next equation:

$$\left(-\frac{\Delta G}{K_B T}\right) = \frac{k_5}{\eta^2} \tag{16}$$

where T is the absolute temperature. The plot ln A *vs* η^{-2} plot, see Figure 7, showed a linear relationship giving a slope of -4.43; the average ΔG calculated was $1.2X10^{-20}$ J $nucleus^{-1}$, where this energy corresponds to the ΔG value requirements for the formation of a stable nucleus (Milchev, 2002).

In the framework of the atomistic theory of electrolytic nucleation, it is possible to estimate the critical size of the Ni nucleus (n_c) from the potential dependence of A through the following equation (Milchev, 1991):

$$n_c = \left(\frac{k_B T}{z e_0}\right)\left(\frac{d \ln A}{d\eta}\right) - \alpha_{Ni} \tag{17}$$

where α_{Ni} is the transfer coefficient for Ni reduction. The plot ln A vs. η showed a linear tendency and a linear relationship, giving a slope of -12.6; see Figure 8. Thus, the critical cluster´s size calculated employing eq. (15) was 0. This result means that each active site on the HOPG electrode surface acts as a critical nucleus (Group, 1985b).

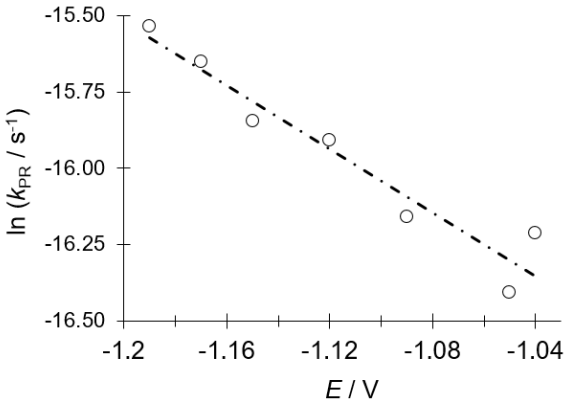

Fig. 9. ln k_{PR} vs -E plots used to calculate the transfer coefficient for proton reduction process The dashed straight line corresponds to linear regression of the experimental data to Equation (16).

The rate constant k_{PR} can also be represented by a Butler–Volmer type relationship, as described in Eq. (16) (Noel & Vasu, 1990), and by examining the slope

of the ln k_{PR} versus E plot in Figure 7, one can estimate the value of α_{PR}. In this study, we found that α_{PR}= 0.07. These values fall within the range reported for the proton reduction process on various substrates (Haghighat & Dawlaty, 2016).

$$k_{PR} = k_{PR}^{0} \exp\left[\frac{-\propto_{PR} zFE}{RT}\right] \quad (18)$$

3.4 Morphological analysis

The morphology of the nickel deposits was studied using Scanning Electron Microscopy (SEM). The micrographs of the deposits formed potentiostatically at -1.090 V are shown in Figures 10a-c. In Figure 10c, it is possible to note that the deposit is characterized by dispersed particles with a spherical structure and diameters ranging from 60 nm to 235 nm. The observed size range could be related to the formation of initial nuclei of different sizes and the evolution of their growth under variable electrochemical conditions, suggesting a progressive nucleation process. Here it is important to mention that in the literature, particles with at least one dimension less than 100 nm are considered as nanoparticles (Kumari & Sarkar, 2021; Szczyglewska, Feliczak-Guzik, & Nowak, 2023) although other authors indicate that this definition is better applicable to nanostructures (Sudha, Sangeetha, Vijayalakshmi, & Barhoum, 2021) or nanomaterials (Baig, Kammakakam, Falath, & Kammakakam, 2021). Thus, the nickel particles observed in Figure 10 may be considered as nanomaterial electrodeposited on HOPG. The particles depicted in Figure 10c were analyzed using Gwyddion software (Nečas & Klapetek, 2012). After filtering, the images were thresholded using the Otsu method to identify the number of particles. The average volume per nucleus was estimated to be 3.05×10^{-15} cm^3, corresponding to a Ni mass of 2.71×10^{-14} g per nucleus, based on nickel's density of 8.9 g cm^{-3}. Considering the last values, the charge associated for electrodeposited nickel nuclei on HOPG electrode at -1.09 V was 0.016 C cm^{-2}. In contrast, the area under the transient curve at -1.09 V was 0.253 C cm^{-2}, indicating that only 6.9% of the applied charge is utilized for nickel electrodeposition, while the remainder is consumed by the proton reduction processes. Note, that these percentages are comparable with those reported in Table 1. Additionally, the observed particle size dispersion may reflect variations in nucleation and growth rates due to strong competition by H^+ by the active sites on the HOPG surface, which may cause the nucleation and growth of Ni particles dispersed.

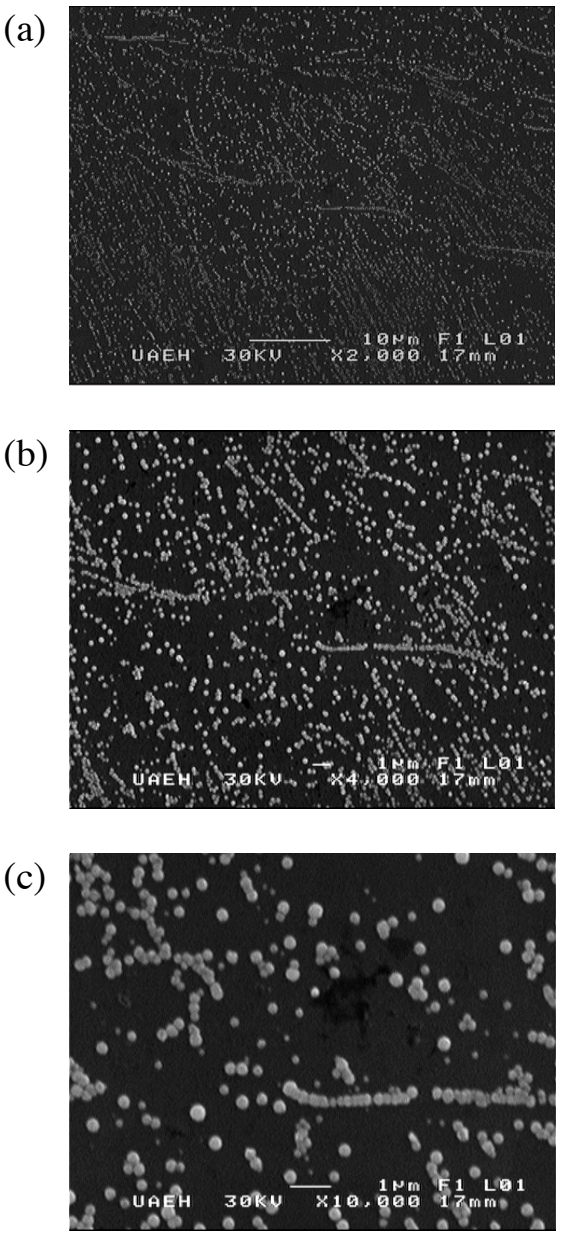

Figure 10. SEM images of the deposits obtained at -1.090 V at different magnifications (a) 2000X, (b) 4000X and (c) 10000X onto the HOPG electrode surface from an aqueous solution of 10^{-2} M of $NiCl_2$ + 0.1 M NH_4Cl.

Conclusion

We have studied Ni electrodeposition onto HOPG from a 10^{-2} M NiCl + 0.1 M NH_4Cl aqueous solution by using voltammetric and potentiostatic techniques. The kinetic analysis revealed a complex nucleation and growth mechanism involving both two-dimensional instantaneous nucleation and three-dimensional nucleation limited by mass transfer together in a proton reduction process. Nucleation parameters such as nucleation rate, density of active

nucleation sites, and saturation nucleus were potential dependent variables. The analysis of current density transients revealed that a significant portion of the applied charge (7.9% on average) is dedicated to the nucleation and growth of nickel, with the remainder primarily supporting proton reduction. The ΔG energy calculated for the formation of a stable nucleus was 1.2×10^{-20} J nucleus^{-1}. The SEM images showed the formation of dispersed particles with a spherical structure and diameters ranging from 60 nm to 235 nm.

Acknowledgements

The author would like to thank to the Universidad Autónoma del Estado de Hidalgo and the computer resources, technical expertise and support provided by the Laboratorio Nacional de Supercómputo del Sureste de México, Consejo Nacional de Ciencia y Tecnología (CONACYT) member of the network of national laboratories and Guanajuato National Laboratory (CONACyT 123732) is acknowledged for the supercomputing resources.

References

Abbott, A. P., Ballantyne, A., Harris, R. C., Juma, J. A., & Ryder, K. S. (2015). A Comparative Study of Nickel Electrodeposition Using Deep Eutectic Solvents and Aqueous Solutions. *Electrochimica Acta*, *176*, 718–726. https://doi.org/10.1016/j.electacta.2015.07.051

Abyaneh, M. Y., Visscher, W., & Barendrecht, E. (1983). Study of the electrocrystallization of nickel by ellipsometry. *Electrochimica Acta*, *28*(3), 285–291. https://doi.org/10.1016/0013-4686(83)85124-X

Alemu, T., Assresahegn, B. D., & Soreta, T. R. (2014). Tuning the Initial Electronucleation Mechanism of Palladium on Glassy Carbon Electrode. *Portugaliae Electrochimica Acta*, *32*(1), 21–33. https://doi.org/10.4152/pea.201401021

Armstrong, R. D., & Harrison, J. A. (1969). Two-Dimensional Nucleation in Electrocrystallization, *236*(1967), 1967–1970.

Baig, N., Kammakakam, I., Falath, W., & Kammakakam, I. (2021). Nanomaterials: A review of synthesis methods, properties, recent progress, and challenges. *Materials Advances*, *2*(6), 1821–1871. https://doi.org/10.1039/d0ma00807a

Bernal Lopez, M., & Ustarroz, J. (2021). Electrodeposition of nanostructured catalysts for electrochemical energy conversion: Current trends and innovative strategies. *Current Opinion in Electrochemistry*, *27*. https://doi.org/10.1016/j.coelec.2021.100688

Berzins, T., & Delahay, P. (1953). Oscillographic Polarographic Waves for the Reversible Deposition of Metals on Solid Electrodes. *Journal of the American Chemical Society*, *75*(3), 555–559. https://doi.org/10.1021/ja01099a013

Cano, C., Romero, E., & Cubillos, G. I. (2023). Improvement of alkyd paints with NiO-ZrO2Y coatings on hot-rolled steel. *Revista Mexicana de Ingeniería Química*, *22*(3), 97–104. https://doi.org/10.24275/rmiq/Proc231

Cheng, Q., Wu, C., Chen, J., Zhou, Y., & Wu, K. (2011). Electrochemical tuning the activity of nickel nanoparticle and application in sensitive detection of chemical oxygen demand. *Journal of Physical Chemistry C*, *115*(46), 22845–22850. https://doi.org/10.1021/JP207442U/ASSET/IMAGES/MEDIUM/JP-2011-07442U_0009.GIF

Cuevas-González, B. G., Monterrubio-Badillo, C., & Cuenca-Álvarez, R. (2018). ELECTRODEPOSITION OF NICKEL IN AN ACIDIC MEDIUM FROM POWDER OF BATTERIES MADE OF NICKEL METAL HYDRIDE (NiMH). *Revista Mexicana de Ingeniería Química*, *17*(2), 603–612. https://doi.org/10.24275/10.24275/uam/izt/dcbi/revmexingquim/2018v17n2/Cuevas

Danaee, I. (2013). 2D–3D nucleation and growth of palladium on graphite electrode. *Journal of Industrial and Engineering Chemistry*, *19*(3), 1008–1013. https://doi.org/10.1016/J.JIEC.2012.11.024

Dean, J, A. (1999). *Handbook of chemistry*. *Soil Science* (Fifteenth). New York: McGraw-Hill, Inc. https://doi.org/10.1016/S0016-0032(40)90947-4

Di Bari, G. A. (2011). Electrodeposition of Nickel. *Modern Electroplating: Fifth Edition*, 79–114. https://doi.org/10.1002/9780470602638.CH3

Dubpernell, G. (2006). Plating & Surface Finishing.Francis, S. (2023). *Nickel plating handbook KNOWLEDGE FOR A BRIGHTER FUTURE*. (Nickel Institute, Ed.) (2022nd ed.). Toronto: Nickel

Institute. Retrieved from https://nickelinstitute.org/media/lxxh1zwr/2023-nickelplatinghandbooka5_printablepdf.pdf

Group, S. E. (1985a). Electrocristallization. In R. Greef, R. Peat, L. M. Peter, D. Pletcher, & J. Robinson (Eds.), *Instrumental Methods in Electrochemistry* (1st ed., Vol. 1, pp. 283–316). Chichester: Woodhead Publishing. Retrieved from http://www.sciencedirect.com:5070/book/9781898563808/instrumental-methods-in-electrochemistry

Group, S. E. (1985b). Electrocristallization. In R. Greef, R. Peat, L. M. Peter, D. Pletcher, & J. Robinson (Eds.), *Instrumental Methods in Electrochemistry* (1st ed., Vol. 1, pp. 283–316).

Chichester: Woodhead Publishing.Grujicic, D., & Pesic, B. (2006). Electrochemical and AFM study of nickel nucleation mechanisms on vitreous carbon from ammonium sulfate solutions. *Electrochimica Acta*, *51*(13), 2678–2690. https://doi.org/10.1016/J.ELECTACTA.2005.08.017

Haghighat, S., & Dawlaty, J. M. (2016). pH Dependence of the Electron-Transfer Coefficient: Comparing a Model to Experiment for Hydrogen Evolution Reaction. *Journal of Physical Chemistry C*, *120*(50), 28489–28496. https://doi.org/10.1021/acs.jpcc.6b10602

Hölzle, M. H., Retter, U., & Kolb, D. M. (1994). The kinetics of structural changes in Cu adlayers on Au(111). *Journal of Electroanalytical Chemistry*, *371*(1–2), 101–109. https://doi.org/10.1016/0022-0728(93)03235-H

Huo, L., Jin, C., Jiang, K., Bao, Q., Hu, Z., & Chu, J. (2022). Applications of Nickel-Based Electrocatalysts for Hydrogen Evolution Reaction. *Advanced Energy and Sustainability Research*, *3*(4), 2100189. https://doi.org/10.1002/AESR.202100189

Jamil, Z., Ruiz-Trejo, E., & Brandon, N. P. (2017). Nickel Electrodeposition on Silver for the Development of Solid Oxide Fuel Cell Anodes and Catalytic Membranes. *Journal of The Electrochemical Society*, *164*(4), D210–D217. https://doi.org/10.1149/2.1081704jes

Jin, C., Zeng, A., Cho, S. J., Nam, S. H., Seo, H. O., Kim, Y. D., & Boo, J. H. (2012). Effect of deposition time and potential on the nucleation and growth of nickel nano particles on nitrogen doped diamond-like carbon thin film. *Thin Solid Films*, *521*, 158–162. https://doi.org/10.1016/J.TSF.2011.12.087

Kireev, S. Y., & Frolov, A. V. (2021). Electrodeposition of Nickel Coatings from Acetate-chloride Electrolyte using Galvanostatic Pulse Electrolysis. *Protection of Metals and Physical Chemistry of Surfaces*, *57*(7), 1375–1379. https://doi.org/10.1134/S2070205121070078/METRICS

Kumari, S., & Sarkar, L. (2021). A Review on Nanoparticles: Structure, Classification, Synthesis & Applications. *Journal of Scientific Research*, *65*(08), 42–46. https://doi.org/10.37398/jsr.2021.650809

Li, G. R., Xu, H., Lu, X. F., Feng, J. X., Tong, Y. X., & Su, C. Y. (2013). Electrochemical synthesis of nanostructured materials for electrochemical energy conversion and storage. *Nanoscale*, *5*(10), 4056–4069. https://doi.org/10.1039/C3NR00607G

Mernissi Cherigui, E. A., Sentosun, K., Bouckenooge, P., Vanrompay, H., Bals, S., Terryn, H., & Ustarroz, J. (2017). Comprehensive Study of the Electrodeposition of Nickel Nanostructures from Deep Eutectic Solvents: Self-Limiting Growth by Electrolysis of Residual Water. *Journal of Physical Chemistry C*, *121*(17), 9337–9347. https://doi.org/10.1021/acs.jpcc.7b01104

Milchev, A. (1991). Electrochemical phase formation on a foreign substrate — basic theoretical concepts and some experimental results Electrochemical phase formation on a foreign substrate-basic theoretical concepts and some experimental results. *Contemporary Physics*, *32*(5), 321–332. https://doi.org/10.1080/00107519108223705

Milchev, A. (2002). *Electrocrystallization. Fundamentals of Nucleation and Growth. Electrocrystallization* (1st ed., Vol. 1). Dordrecht: Kluwer Academic Publishers. https://doi.org/10.1007/B113784

Mostany, J., Mozota, J., & Scharifker, B. R. (1984). Three-dimensional nucleation with diffusion controlled growth: Part II. The nucleation of lead on vitreous carbon. *Journal of Electroanalytical Chemistry and Interfacial Electrochemistry*, *177*(1–2), 25–37. https://doi.org/10.1016/0022-0728(84)80208-9

Nečas, D., & Klapetek, P. (2012). Gwyddion: An open-source software for SPM data

analysis. *Central European Journal of Physics*, *10*(1), 181–188. https://doi.org/10.2478/S11534-011-0096-2/MACHINEREADABLECITATION/RIS

Ni, X., Zhang, Y., Wang, C., Hong, Y., Chen, Y., Su, Y., … Du, Y. (2022). Mechanism and Application of Nickel NanoCone by Electrodeposition on a Flexible Substrate Abstract :, *28*(7), 1–11. https://doi.org/10.13208/j.electrochem.2213008Noel, M., & Vasu, K. I. (1990). *Cyclic Voltammetry and the Frontiers of Electrochemistry*. (Aspect publications, Ed.). London: Aspect. Retrieved from https://books.google.com.mx/books?id=L4IvAQAAIAAJ

Palomar-Pardavé, M., Scharifker, B. R., Arce, E. M., & Romero-Romo, M. (2005). Nucleation and diffusion-controlled growth of electroactive centers: Reduction of protons during cobalt electrodeposition. *Electrochimica Acta*, *50*(24), 4736–4745. https://doi.org/10.1016/J.ELECTACTA.2005.03.004

Putri, Y. M. T. A., Syauqi, M. I., Rahmawati, I., Aliyah, A., Sanjaya, A. R., & Ivandini, T. A. (2024). Advancements in Ni-based Catalysts for Direct Urea Fuel Cells: A Comprehensive Review. *ChemElectroChem*, *11*(5), e202300637. https://doi.org/10.1002/CELC.202300637

Rehman, Z. U., Nawaz, M., Ullah, H., Uddin, I., Shad, S., Eldin, E., … Javed, M. S. (2022). Synthesis and Characterization of Ni Nanoparticles via the Microemulsion Technique and Its Applications for Energy Storage Devices. *Materials 2023, Vol. 16, Page 325*, *16*(1), 325. https://doi.org/10.3390/MA16010325

Rios-Reyes, C. H., Mendoza-Huizar, L. H., & Rivera, M. (2010). Electrochemical kinetic study about cobalt electrodeposition onto GCE and HOPG substrates from sulfate sodium solutions. *Journal of Solid State Electrochemistry 2009 14:4*, *14*(4), 659–668. https://doi.org/10.1007/S10008-009-0816-3

Ruiz-Vela, J. I., Rodríguez-Vázquez, E. E., Gudiño-Pérez, Y., Sánchez-Ramírez, R., & Montes-Rodríguez, J. J. (2023). Effect of complexing/buffering agent on the characteristics of a high phosphorous electroless nickel coating. *Revista Mexicana de Ingeniería Química*, *22*(2), 1–10. https://doi.org/10.24275/rmiq/Proc2331

Scharifker, B., & Hills, G. (1983). Theoretical and experimental studies of multiple nucleation. *Electrochimica Acta*, *28*(7), 879–889. https://doi.org/10.1016/0013-4686(83)85163-9

Serruya, A., Mostany, J., & Scharifker, B. R. (1999). The kinetics of mercury nucleation from Hg22+ and Hg2+ solutions on vitreous carbon electrodes. *Journal of Electroanalytical Chemistry*, *464*(1), 39–47. https://doi.org/10.1016/S0022-0728(98)00464-1

Skibińska, K., Semeniuk, S., Kutyła, D., Jędraczka, A., & Zabiński, P. (2021). Study on Synthesis and Modification of Conical Ni Structures by One-Step Method, *66*, 861–869. https://doi.org/10.24425/amm.2021.136391

Sotskaya, N. V., Sapronova, L. V., & Dolgikh, O. V. (2014). Kinetics of the nucleation and growth of nickel particles in α-alanine-containing electrolytes. *Protection of Metals and Physical Chemistry of Surfaces*, *50*(1), 22–26. https://doi.org/10.1134/S2070205114010134

Sudha, P. N., Sangeetha, K., Vijayalakshmi, K., & Barhoum, A. (2021). *Chapter 12 - Nanomaterials history, classification, unique properties, production and market*. *Emerging Applications of Nanoparticles and Architecture Nanostructures*. Elsevier Inc. https://doi.org/10.1016/B978-0-323-51254-1/00012-9

Szczyglewska, P., Feliczak-Guzik, A., & Nowak, I. (2023). Nanotechnology–General Aspects: A Chemical Reduction Approach to the Synthesis of Nanoparticles. *Molecules*, *28*(13). https://doi.org/10.3390/molecules28134932

Tafel, J. (1905). Julius Tafel. *Society, Journal of the Chemical*, *88*, 668–676.Torabi, M., & Dolati, A. (2010). A kinetic study on the electrodeposition of nickel nanostructure and its electrocatalytic activity for hydrogen evolution reaction. *Journal of Applied Electrochemistry*, *40*(11), 1941–1947. https://doi.org/10.1007/S10800-010-0170-2/METRICS

Vij, V., Sultan, S., Harzandi, A. M., Meena, A., Tiwari, J. N., Lee, W. G., … Kim, K. S. (2017). Nickel-based electrocatalysts for energy-related applications: Oxygen reduction, oxygen evolution, and hydrogen evolution reactions. *ACS Catalysis*, *7*(10), 7196–7225. https://doi.org/10.1021/acscatal.7b01800

Wang, Y., Williamson, N., Dawson, R., & Bimbo, N. (2023). Electrodeposition of nickel–iron on stainless steel as an efficient electrocatalyst coating for the oxygen evolution reaction

in alkaline conditions. *Journal of Applied Electrochemistry*, *53*(5), 877–892. https://doi.org/10.1007/S10800-022-01817-4/FIGURES/8

Whiston, M. M., Bilec, M. M., & Schaefer, L. A. (2015). Influence of the charge double layer on solid oxide fuel cell stack behavior. *Journal of Power Sources*, *293*, 767–777. https://doi.org/10.1016/j.jpowsour.2015.05.085

Zheng, G. Q., Cao, H. Z., & Zheng, L. F. (2007). Influence of ammonia concentration on anodic deposition of nickel oxide. *Journal of Applied Electrochemistry*, *37*(7), 799–803. https://doi.org/10.1007/S10800-007-9313-5/METRICS

Zhu, Y. L., Katayama, Y., & Miura, T. (2014). Effects of coumarin and saccharin on electrodeposition of Ni from a hydrophobic ionic liquid. *Electrochimica Acta*, *123*, 303–308. https://doi.org/10.1016/J.ELECTACTA.2013.12.181